Chiral two-dimensional electron gas in a periodic magnetic field: Persistent current and quantized anomalous Hall effect

M. Taillefumier,[1,2,3] V. K. Dugaev,[4,5] B. Canals,[2] C. Lacroix,[2] and P. Bruno[1,6]
[1]*Max-Planck-Institut für Mikrostrukturphysik, Weinberg 2, 06120 Halle, Germany*
[2]*Institut Néel, CNRS/UJF, 25 Avenue des Martyrs, BP 166, 38042 Grenoble Cedex 09, France*
[3]*Department of Physics, Norwegian University of Science and Technology, N-7491 Trondheim, Norway*
[4]*Department of Physics, Rzeszów University of Technology, al. Powstańców Warszawy 6, 35-959 Rzeszów, Poland*
[5]*Department of Physics and CFIF, Instituto Superior Técnico, Universidade Técnica de Lisboa, Avenue Rovisco Pais, 1049-001 Lisbon, Portugal*
[6]*European Synchrotron Radiation Facility, BP 220, 38043 Grenoble Cedex, France*
(Received 28 January 2008; revised manuscript received 2 September 2008; published 31 October 2008)

We study the energy spectrum and electronic properties of two-dimensional electron gas in a periodic magnetic field of zero average with symmetry of triangular lattice. We demonstrate how the structure of electron energy bands can be changed with the variation in the field strength so that we can start from nearly free-electron gas and then transform it continuously to a system of essentially localized chiral electron states. We find that the electrons near some minima of the effective potential are responsible for occurrence of dissipationless persistent currents creating a lattice of current contours. The topological properties of the electron energy bands are also varied with the intensity of periodic field. We calculated the topological Chern numbers of several lower-energy bands as a function of the field. The corresponding Hall conductivity is nonzero, and when the Fermi level lies in the gap, it is quantized.

DOI: 10.1103/PhysRevB.78.155330 PACS number(s): 73.21.−b, 73.50.Jt, 75.47.−m, 73.23.Ra

I. INTRODUCTION

The aim of this work is to study the effect of a periodic magnetic field of zero average on the dynamic of a free-electron gas. The magnetic-field distribution forms a "magnetic-field lattice" for electrons, which results in the formation of electron energy bands controlled by the strength and the geometry of the magnetic field.

The possibility of using periodic magnetic fields for tailoring the electronic structure is mostly related to recent advances in nanotechnology, which enable to manufacture two-dimensional (2D) lattice of ferromagnetic nanocylinders.[1] This idea has been already used by us to suggest a system where the spin chirality mechanism related to the anomalous Hall effect (AHE) in frustrated ferromagnets[2–5] can be measured and controlled externally.[6] To detect this effect, we proposed to measure the Hall effect in 2D diluted magnetic semiconductor on top of the nanolattice of ferromagnetic cylinders. Another possible way to create the periodic field is to use an array of magnetic nanodots with tunable out-of-plane magnetization like in Ref. 7.

Previous investigations of the 2D electronic system in periodic magnetic fields concentrated mostly on the one-dimensional (1D) periodic modulation[8,9] and, in some cases, on a mutual effect of the uniform and periodic magnetic fields.[10–14] The main difference of our work is that we assume that the uniform magnetic field is exactly zero, whereas the periodic field forms a real two-dimensional nanolattice. For definiteness, here we focus on the case of triangular lattice, which corresponds to the nanocylinder structure in Ref. 1. It should be emphasized that the assumption of zero uniform field is very important because it results in formation of well-defined electron energy bands characterized by the electron momentum **k** such as in the case of electric modulation. On the other hand, the presence of 2D magnetic-field modulation substantially changes a picture of the "snakelike" electron motion in a nonuniform (linear-in-gradient) magnetic field.[15]

The semiclassical consideration of the motion of electrons in inhomogeneous magnetic field shows that the low-energy electrons mostly tend to localize near the lines of zero magnetic field.[15,16] The corresponding effective potential has a different form for electrons moving in opposite directions along the zero-field line. We found an analogous tendency to the localization of electrons in the 2D periodic field. In this case, the zero-field lines correspond to some closed trajectories of electron motion, which is chiral and quantized and which leads to occurrence of equilibrium *persistent currents*. It should be noted that usually the persistent currents are associated with mesoscopic rings, for which the symmetry of the electron motion in opposite directions is broken by the magnetic field.[17–22] However, in our case of the "magnetic crystal," the persistent currents appear similar to a periodic array of circular currents.

Quite recently a lot of discussions have been induced by the study of an "intrinsic" mechanism of AHE.[23,24] In the ballistic regime, when the impurities can be totally neglected, the anomalous Hall effect is related to the topology of electron energy bands, which can be characterized by integers called Chern numbers. It turned out that the discussion of the intrinsic mechanism of AHE lead to a partial revision of the Landau theory of Fermi liquid because the transport properties are found to be related to the Berry curvature of electron bands in momentum space,[25] which means that the corresponding topological element should be added to the Landau theory.[26]

Some rather simplified theoretical models such as the 2D electron gas with Rashba spin-orbit interaction or the relativ-

istic 2D Dirac model allow full analytical calculation of the Berry curvatures and Chern numbers. Recently, several publications reported calculations of the Berry curvature for $SrRuO_3$ (Ref. 24) and bcc Fe (Refs. 27 and 28) using *ab initio* methods. In our previous paper,[29] we presented numerical calculations of the Berry curvature of the energy bands of electrons interacting with a chiral spin texture defined on top of a kagomé lattice. However, in the latter case the essential element is the inhomogeneous orientation of the localized spins, which leads to the chirality contribution[2–5] to the AHE.

In this paper, we study the topology of electron energy bands by calculating the Chern numbers as a function of the intensity of periodic magnetic field. The model with a periodic field gives us such a parameter, which can presumably be varied in the experiment (for example, by changing a distance between the 2D layer and the nanocylinder lattice). This way we can demonstrate a strong jumplike dependence of the Chern numbers on the field.

II. MODEL

We consider a model of two-dimensional electron gas (2DEG) of spinless electrons in the x-y plane under periodic magnetic field $\mathbf{B}(\mathbf{r})$. Since the electrons move in the plane, the only component of field acting on electrons is the component perpendicular to this plane, which we denote by $B(\mathbf{r})$. Then the properties of the system can be described by the following Hamiltonian:

$$\mathcal{H} = \frac{\hbar^2}{2m}\left(-i\nabla - \frac{e}{\hbar c}\mathbf{A}(\mathbf{r})\right)^2, \tag{1}$$

where m is the effective electron mass and $\mathbf{A}(\mathbf{r})$ is the vector potential related to the magnetic field $B(\mathbf{r})$ by $\nabla \times A(\mathbf{r}) = B(\mathbf{r})$. In the following we use the Coulomb gauge determined by the condition $\nabla \cdot \mathbf{A}(\mathbf{r}) = 0$. In the case of zero average field, it is possible to choose the vector potential $\mathbf{A}(\mathbf{r})$ as periodic in space (see below).

Thus, we have a problem of electron in a periodic potential, and we can use the Bloch theorem for the eigenfunctions of Hamiltonian (1),

$$\psi_{n,\mathbf{k}}(\mathbf{r}) = e^{i\mathbf{k}\cdot\mathbf{r}} u_{n,\mathbf{k}}(\mathbf{r}), \tag{2}$$

where n is the band index and $\mathbf{k}$ is the crystal momentum, which is restricted to the first Brillouin zone. The function $u_{n,\mathbf{k}}(\mathbf{r})$ is periodic, $u_{n,\mathbf{k}}(\mathbf{r}) = u_{n,\mathbf{k}}(\mathbf{r}+\mathbf{R})$, with $\mathbf{R}$ being the lattice vector determined by the periodicity of the potential. Substituting Eq. (2) into Eq. (1), we find that $u_{n,\mathbf{k}}(\mathbf{r})$ verify

$$\mathcal{H}_{\mathbf{k}} u_{n,\mathbf{k}}(\mathbf{r}) = \varepsilon_{n,\mathbf{k}} u_{n,\mathbf{k}}(\mathbf{r}), \tag{3}$$

where $\varepsilon_{n,\mathbf{k}}$ is the eigenvalue associated with the eigenfunction $\psi_{n,\mathbf{k}}(\mathbf{r})$, and

$$\mathcal{H}_{\mathbf{k}} = \frac{\hbar^2}{2m}\left(-i\nabla + \mathbf{k} - \frac{e}{\hbar c}\mathbf{A}(\mathbf{r})\right)^2 \tag{4}$$

is the reduced Hamiltonian depending on $\mathbf{k}$. Using the periodicity of $u_{n,\mathbf{k}}(\mathbf{r})$, we can write it as

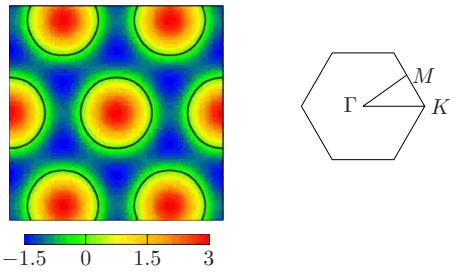

FIG. 1. (Color online) (Left panel) Density plot of the magnetic-field distribution (in arbitrary units). The black lines are the isolines $B(\mathbf{r})=0$. (Right panel) First Brillouin zone of the triangular lattice.

$$u_{n,\mathbf{k}}(\mathbf{r}) = \sum_{\mathbf{g}} u_{n,\mathbf{k}}(\mathbf{g}) e^{i\mathbf{g}\cdot\mathbf{r}}, \tag{5}$$

where $\mathbf{g}$ is a vector of the reciprocal lattice, $u_{n,\mathbf{k}}(\mathbf{g})$ is the Fourier transform of $u_{n,\mathbf{k}}(\mathbf{r})$ defined by

$$u_{n,\mathbf{k}}(\mathbf{g}) = \frac{1}{S}\int_s u_{n,\mathbf{k}}(\mathbf{r}) e^{-i\mathbf{g}\cdot\mathbf{r}} d^2\mathbf{r}, \tag{6}$$

and S is the area of the unit cell. Substituting Eq. (6) into Eq. (3), we find that $u_{n,\mathbf{k}}(\mathbf{g})$ satisfy the following set of equations:

$$\sum_{\mathbf{g}'} \mathcal{H}_{\mathbf{k}}(\mathbf{g},\mathbf{g}') u_{n,\mathbf{k}}(\mathbf{g}') = \varepsilon_{n,\mathbf{k}} u_{n,\mathbf{k}}(\mathbf{g}). \tag{7}$$

The matrix elements $\mathcal{H}_{\mathbf{k}}(\mathbf{g},\mathbf{g}')$ can be calculated by using Eqs. (4) and (5),

$$\mathcal{H}_{\mathbf{k}}(\mathbf{g},\mathbf{g}') = \frac{\hbar^2}{2m}\left[(\mathbf{k}+\mathbf{g})^2 \delta_{\mathbf{g},\mathbf{g}'} - \frac{2e}{\hbar c}(\mathbf{k}+\mathbf{g})\cdot\mathbf{A}(\mathbf{g}-\mathbf{g}') + \frac{e^2}{\hbar^2 c^2}\mathbf{A}^2(\mathbf{g}-\mathbf{g}')\right], \tag{8}$$

where $\mathbf{A}(\mathbf{g})$ and $\mathbf{A}^2(\mathbf{g})$ are the Fourier transforms of $\mathbf{A}(\mathbf{r})$ and $\mathbf{A}^2(\mathbf{r})$, respectively. Note that Eq. (8) depends on the gauge and is written in the Coulomb gauge $\mathbf{g}\cdot\mathbf{A}(\mathbf{g})=0$. Finally, the Fourier transform of $\mathbf{A}^2(\mathbf{r})$ is related to $\mathbf{A}(\mathbf{g})$ by the convolution,

$$\mathbf{A}^2(\mathbf{g}) = \sum_{\mathbf{g}'} \mathbf{A}(\mathbf{g}-\mathbf{g}')\cdot\mathbf{A}(\mathbf{g}). \tag{9}$$

Up to now, the derivation is quite general. In the following, we specify the form of the magnetic-field profile to the symmetry of triangular lattice. It can be realized by using a periodic array of ferromagnetic nanocylinders with a period of few ten nanometers[1] on top of 2DEG, similar to that explained in Ref. 6. This distribution is periodic in plane and its Fourier components are decreasing exponentially with the wave vector $\mathbf{g}$ and with the distance between the 2D film and the array of ferromagnetic nanocylinders.

The magnetic field has a zero net flux over the unit cell, and we assume that only the first Fourier components of the field are important. The magnetic-field profile is shown in Fig. 1. Our approximation is valid when the distance be-

tween the 2DEG and the array of ferromagnetic nanocylinders is of the order of the lattice period.

We write down the z component of the magnetic field as

$$B(\mathbf{r}) = B_0\left[\cos\left(\frac{2\pi}{a}\mathbf{b}_1\cdot\mathbf{r}\right)+\cos\left(\frac{2\pi}{a}\mathbf{b}_2\cdot\mathbf{r}\right)+\cos\left(\frac{2\pi}{a}\mathbf{b}_3\cdot\mathbf{r}\right)\right], \tag{10}$$

where B_0 is the amplitude of the field and a is the lattice period. The vectors $\mathbf{b}_i$ with $i=1,2$ and $\mathbf{b}_3=\mathbf{b}_2+\mathbf{b}_1$ are the vectors of reciprocal lattice of the triangular lattice. They are defined by the relations $\mathbf{b}_i\cdot\mathbf{a}_j=\delta_{ij}$, where $i,j=1,2$, $\mathbf{a}_1=(1,0)$, $\mathbf{a}_2=(1/2,\sqrt{3}/2)$, and $\mathbf{a}_3=\mathbf{a}_2-\mathbf{a}_1$. The first Brillouin zone (Fig. 1) is a hexagon with corners at $\mathbf{k}_i=\frac{4\pi}{3a}\mathbf{a}_i$. The (Coulomb gauge) vector potential $\mathbf{A}(\mathbf{r})$ can be chosen in the following form (i.e., periodic in space):

$$\mathbf{A}(\mathbf{r}) = A_0\left[\mathbf{a_2}\sin\left(\frac{2\pi}{a}\mathbf{b}_1\cdot\mathbf{r}\right)-\mathbf{a}_1\sin\left(\frac{2\pi}{a}\mathbf{b}_2\cdot\mathbf{r}\right)+\mathbf{a}_3\sin\left(\frac{2\pi}{a}\mathbf{b}_3\cdot\mathbf{r}\right),\right] \tag{11}$$

where $A_0=B_0\sqrt{3}a/4\pi$.

For the numerical calculations we define the reduced units $B(\mathbf{r})\to B_0B(\mathbf{r})$, $\mathbf{A}(\mathbf{r})\to A_0\mathbf{A}(\mathbf{r})$, $\mathbf{g}\to\frac{2\pi}{a}\mathbf{g}$ is the vector of reciprocal lattice, and $\mathbf{k}\to\frac{2\pi}{a}\mathbf{k}$ is the crystal momentum taken in the first Brillouin zone. The energy ε is replaced by $\varepsilon\to\varepsilon_0\varepsilon$, with $\varepsilon_0=\hbar^2/2ma^2$. Finally, after introducing the dimensionless parameter $\alpha=-eA_0a/\mathrm{H.c.}$, Eq. (8) becomes

$$\mathcal{H}_{\mathbf{k}}(\mathbf{g},\mathbf{g}') = \varepsilon_0[(\mathbf{k}+\mathbf{g})^2\delta_{\mathbf{g},\mathbf{g}'}+2\alpha\mathbf{A}(\mathbf{g}-\mathbf{g}')\cdot(\mathbf{k}+\mathbf{g})+\alpha^2\mathbf{A}^2(\mathbf{g}-\mathbf{g}')] \tag{12}$$

so that, unless stated, all the quantities will be presented in the reduced dimensionless units. In what follows α is the main parameter determining the intensity of the magnetic-field modulation.

III. ELECTRON ENERGY SPECTRUM AND WAVE FUNCTIONS

A. Weak magnetic field: Perturbation theory

Due to our choice of the gauge for the vector potential, Eq. (11), one can use the perturbation theory over $\mathbf{A}(\mathbf{r})$, which corresponds to the limit of weak magnetic field. Then the unperturbed Hamiltonian is $\mathcal{H}_0=-\hbar^2\nabla^2/2m$ (in this section we do not use reduced units), and the Hamiltonian of interaction,

$$\mathcal{H}_{\mathrm{int}} = \frac{ie\hbar}{mc}\mathbf{A}(\mathbf{r})\cdot\nabla+\frac{e^2}{2mc^2}\mathbf{A}^2(\mathbf{r}), \tag{13}$$

with

$$\mathbf{A}(\mathbf{r}) = \mathbf{A}_2\sin(\mathbf{g}_1\cdot\mathbf{r})-\mathbf{A}_1\sin(\mathbf{g}_2\cdot\mathbf{r})+\mathbf{A}_3\sin(\mathbf{g}_3\cdot\mathbf{r}), \tag{14}$$

where $\mathbf{A}_i=A_0\mathbf{a}_i$ and $\mathbf{g}_i=\frac{2\pi}{a}\mathbf{b}_i$. The eigenfunctions of $\mathcal{H}_0$ are the usual plane waves $\psi_{\mathbf{k}}(\mathbf{r})=\frac{1}{2\pi}e^{i\mathbf{k}\cdot\mathbf{r}}$, and the corresponding matrix elements of interaction can be calculated as the Fourier components of $\mathcal{H}_{\mathrm{int}}$,

$$\begin{aligned}\mathcal{H}_{\mathrm{int}}(\mathbf{q}) = \frac{e^2A_0^2}{8mc^2}[&6\delta(\mathbf{q})-\delta(\mathbf{q}+2\mathbf{g}_1)-\delta(\mathbf{q}-2\mathbf{g}_1)-\delta(\mathbf{q}+2\mathbf{g}_2)\\&-\delta(\mathbf{q}-2\mathbf{g}_2)-\delta(\mathbf{q}+2\mathbf{g}_3)-\delta(\mathbf{q}-2\mathbf{g}_3)\\&+\delta(\mathbf{q}+\mathbf{g}_1+\mathbf{g}_2)-\delta(\mathbf{q}+\mathbf{g}_1-\mathbf{g}_2)-\delta(\mathbf{q}-\mathbf{g}_1+\mathbf{g}_2)\\&+\delta(\mathbf{q}-\mathbf{g}_1-\mathbf{g}_2)-\delta(\mathbf{q}+\mathbf{g}_1+\mathbf{g}_3)+\delta(\mathbf{q}+\mathbf{g}_1-\mathbf{g}_3)\\&+\delta(\mathbf{q}-\mathbf{g}_1+\mathbf{g}_3)-\delta(\mathbf{q}-\mathbf{g}_1-\mathbf{g}_3)-\delta(\mathbf{q}+\mathbf{g}_2+\mathbf{g}_3)\\&+\delta(\mathbf{q}+\mathbf{g}_2-\mathbf{g}_3)+\delta(\mathbf{q}-\mathbf{g}_2+\mathbf{g}_3)-\delta(\mathbf{q}-\mathbf{g}_2-\mathbf{g}_3)].\end{aligned} \tag{15}$$

It should be noted that any matrix elements of the first (linear in $\mathbf{A}$) term in Eq. (13) are zero.

The perturbation related to $\mathcal{H}_{\mathrm{int}}$ breaks the degeneracy of states belonging to the points in the Brillouin zone separated by vector $\mathbf{g}$, for which $\mathcal{H}_{\mathrm{int}}(\mathbf{g})\neq 0$. Using Eq. (15) we find the matrix elements corresponding to transitions between the states in the opposite points at the Brillouin-zone edges,

$$\mathcal{H}_{\mathrm{int}}(\mathbf{g}_1)=\mathcal{H}_{\mathrm{int}}(\mathbf{g}_2)=\mathcal{H}_{\mathrm{int}}(\mathbf{g}_3)=\frac{e^2A_0^2}{8mc^2}. \tag{16}$$

For example, the element $\mathcal{H}_{\mathrm{int}}(\mathbf{g}_2)$ couples the degenerate states $\mathbf{k}=(0,-2\pi/a\sqrt{3})$ and $\mathbf{k}'=(0,2\pi/a\sqrt{3})$. Using the perturbation theory for the degenerate states $\mathbf{k}$ and $\mathbf{k}'$, we can find that the value $e^2A_0^2/8mc^2$ determines the magnitude of the corresponding energy gap at the Brillouin-zone edge. Note that the gap in these points is nonzero for any weak perturbation, and it increases with the amplitude of magnetic field as B_0^2.

We can find that the perturbation theory approach is valid for $|\alpha|\ll 1$. This condition can be also presented as $\phi/\phi_0\ll 1$, where $\phi=B_0a^2\sqrt{3}/2$ is the flux of field B_0 per elementary cell and $\phi_0=\mathrm{h}c/e$ is the flux quantum.

B. Energy spectrum

1. Degeneracies and symmetries of the Hamiltonian

The Hamiltonian (1) is invariant under discrete translations of vectors $\mathbf{R}=i\mathbf{a}_1+j\mathbf{a}_2$ and because of the polar nature of the vector potential $\mathbf{A}(\mathbf{r})$, it is also invariant under the point group C_6 (but not C_{6v}) of pure sixfold rotations. Its space group is therefore Abelian, and its irreducible representations are all of dimension 1. This physically means that the energy spectrum can only have accidental degeneracies between consecutive energy bands.

2. Energy spectrum: Numerical results

The solution of Eq. (1) should be obtained by diagonalizing the infinite matrix with elements given by Eq. (8). In practice, one cuts the basis to get a finite matrix. We cut the basis by introducing the energy cutoff ε_c; i.e., we keep the plane waves with energies $\varepsilon\leq\varepsilon_c$ and neglect the others. Then we diagonalize the obtained matrix by using the Lanczos algorithm (with reorthogonalization) implemented in the

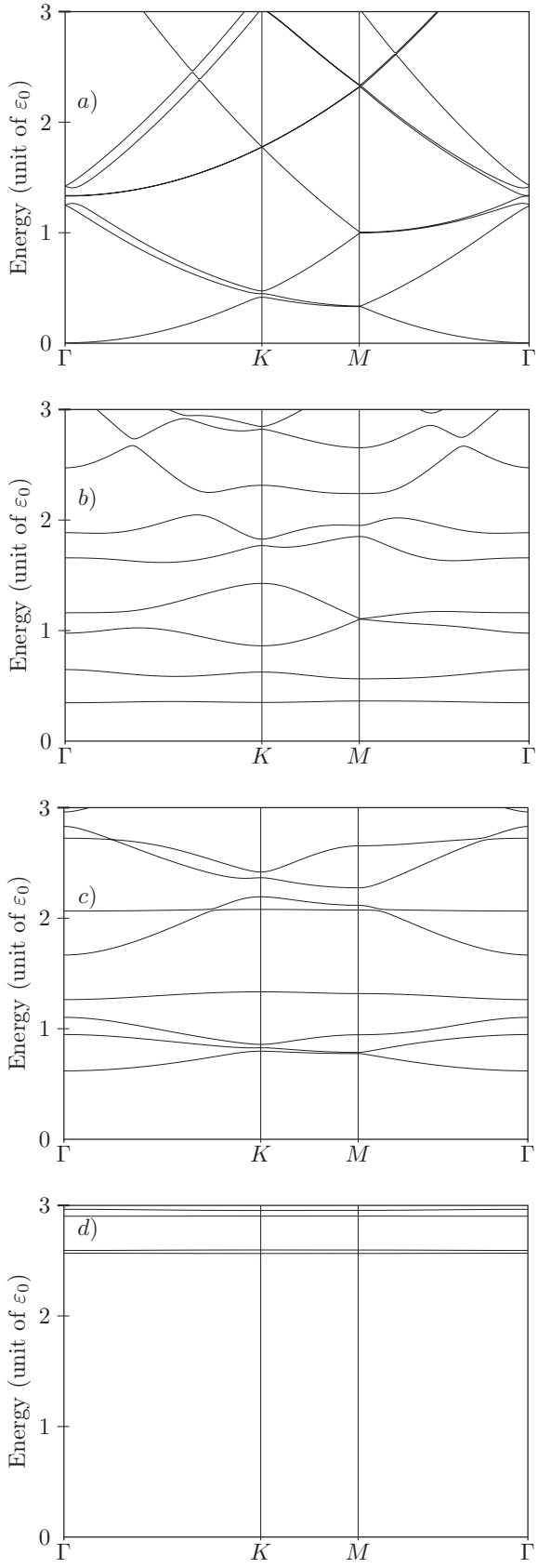

FIG. 2. Energy spectrum of electrons in periodic magnetic field calculated for (a) $\alpha=0.05$, (b) 0.5, (c) 1, and (d) 5. Local gaps are open at points of the Brillouin zone where degeneracies due to the Bragg plan are located.

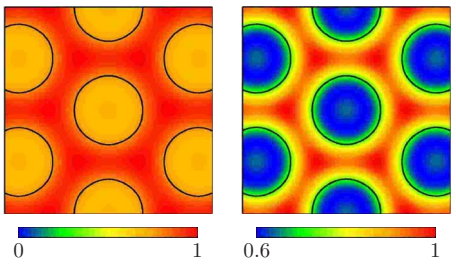

FIG. 3. (Color online) Probability distribution for the Bloch states of the first energy band in Γ point for $\alpha=0.5$. The black lines are the isolines of constant magnetic field $B(\mathbf{r})=0$. The left panel shows that the particle is substantially delocalized over the unit cell but avoids the regions where the magnetic field is maximum. This effect can clearly be seen on the right panel where the color scale has been changed in order to see better the fine structure of the Bloch states.

library SLEPC.[30] Finally, the value of ε_c is chosen to get the converged quantities.

The presence of linear term, which couples the momentum $\mathbf{k}$ to the vector potential, gives rise to a rich energy spectrum when the amplitude of magnetic field is changed. In the low-field regime the band structure [Fig. 2(a)] is similar to the band structure of free particle. It is slightly modified near the points obeying relation $\mathbf{k}^2=(\mathbf{k}+\mathbf{g})^2$ because the Bloch bands are degenerated at these points. As we found in Secs. III A and III B 1, the application of a periodic vector potential leaves the degeneracy.

The energy spectrum demonstrates a strong variation when the amplitude of magnetic field is increased. The gaps can be seen for rather weak values of $|\alpha|$ [Fig. 2(b)] and the band width continuously decreases when $|\alpha|$ increases. Figures 2(b) and 2(c) show that the band crossing occur at some high-symmetry points of the first Brillouin zone such as the points K, M, and Γ. We see that the band crossing occur very often when $|\alpha|$ is increased. As we shall see later, this property is important for the quantization of Hall conductivity because it gives rise to the jumps in σ_{xy}. The corresponding jumps of σ_{xy} when an external parameter is changed can be identified as *topological transitions*.

Finally, for larger values of $|\alpha|$ [Fig. 2(d)], the bands are practically flat indicating that (i) electrons are mostly localized and (ii) they have very low group velocity (i.e., the electrons are extremely heavy).

C. Properties of the Bloch states

Here we present the probability distribution of the Bloch states in dependence on the parameter α. Our study is restricted to the high-symmetry points of the first Brillouin zone, where the Bloch state $u_{n,\mathbf{k}}(\mathbf{r})$ has the symmetry of the point $\mathbf{k}$.

Let us start by considering the Γ point. The Bloch state at this point has the symmetry of the lattice. We consider first the band $n=1$ as a function of α. The results of calculation of the probability distribution $|\psi_{n,\mathbf{k}}(\mathbf{r})|^2$ for $\alpha=0.5$ are presented in Fig. 3. At small $|\alpha|$ (see Fig. 3, left), the electrons are mainly delocalized over the unit cell. However, they avoid

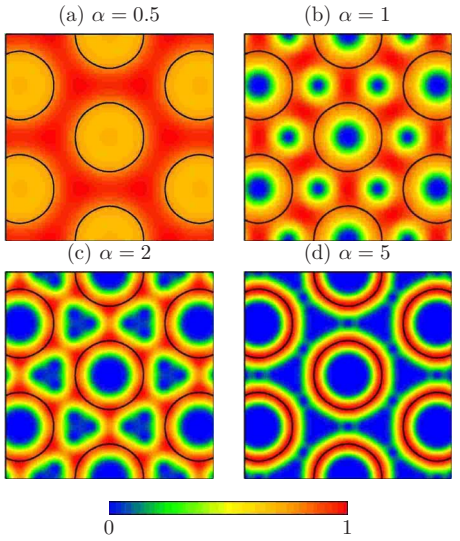

FIG. 4. (Color online) Bloch states of the first band in the Γ point for (a) α=0.5, (b) 1, (c) 2, and (d) 5. The black lines correspond to $B(\mathbf{r})=0$. These figures shows that the particle tries to avoid the region where the magnetic field is large. This effect can be seen already in figure (a), but it is better visible in (b) and (c). For larger $|\alpha|$, the particle is confined around the lines of zero magnetic field.

the regions where the magnetic field is large (inside the regions delimited by the black lines on the figure). This is also clearly illustrated by Fig. 3, right, where the color scale has been changed in order to see the fine structure of the distribution. As shown in Fig. 4(b), the increase in the parameter $|\alpha|$ enhances this effect. The particles are rejected from the region where the magnetic field is large and concentrated in the regions where the field is close to zero [Figs. 4(b) and 4(c)]. Figure 4(d) represents the limiting case where the repulsion effect confines the particle to the region close to the line of $B(\mathbf{r})=0$ [black lines in Fig. 4(d)]. In this case, the particle is moving in an effective potential created by the field profile, which forms a ring, with the ring width depending on α.

This behavior corresponds to the semiclassical picture of the electron motion in linear magnetic field.[15] In this approach the low-energy electron drifts along the line of minimum magnetic field, and the trajectory of this motion can be wavy or snakelike depending on the drift direction. One can also understand the effect of electron localization as a tendency to occupy the region, in which the energy of Landau level is minimum.

Up to now, we considered the states in which the particle is rejected into the regions of the weak field, but one can also obtain the states with particles rejected from these regions and concentrated in the regions where $B(\mathbf{r})$ is large. Such situation can be found by considering higher-energy bands. A typical example is presented in the right panel of Fig. 5.

We also calculated the probability distribution at other symmetry points of the Brillouin zone. Except for a partial loss of symmetry, these electronic states have properties similar to the electronic states at the Γ point.

Our main result for this section is that the strong periodic field results in localization of electrons in some low-energy

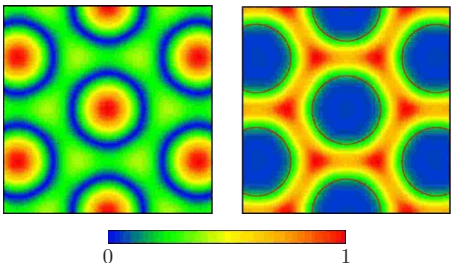

FIG. 5. (Color online) Bloch states of the fifth band (α=0.5) and fourth band (α=1) in the Γ point. The particle is confined in the regions of strong magnetic field.

states. The electrons of the lowest-energy bands are effectively confined within some rings near the closed lines of zero magnetic field, and the rings form a regular array corresponding to the symmetry of the magnetic-field lattice. The characteristic thickness of the rings decreases with the field intensity.

IV. PERSISTENT CURRENTS

Now we show that the electrons, which are confined within the rings, are moving along the zero-field lines creating a regular array of equilibrium persistent currents. For this purpose we calculate the local current density $\mathbf{J}_{n,\mathbf{k}}(\mathbf{r})$ defined as

$$\mathbf{J}_{n,\mathbf{k}}(\mathbf{r}) = \frac{\hbar}{2m}\mathrm{Re}\left[u^{\dagger}_{n,\mathbf{k}}(\mathbf{r})\left(-i\nabla + \mathbf{k} - \frac{e}{\hbar}\mathbf{A}(\mathbf{r})\right)u_{n,\mathbf{k}}(\mathbf{r})\right], \tag{17}$$

where $u_{n,\mathbf{k}}(\mathbf{r})$ refers to the corresponding Bloch state. One can also calculate the total current density $\mathbf{J}(\mathbf{r})$ defined as the sum over all occupied states below the Fermi level ε_F.

Let us consider the current distribution at the Γ point for α=5 and n=1. The distribution density for the corresponding Bloch state is shown in Fig. 4(d), whereas Fig. 6 represents the spatial distribution of x and y components of current density [Eq. (17)]. As we see from Fig. 6, the electrons within the rings are moving along the lines of $B(\mathbf{r})=0$ (black lines on the figure) so that the current density is nonzero along the circle. One can see at this picture that the current density has an oscillating fine structure in the direction per-

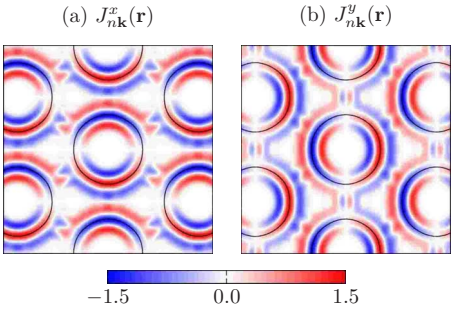

FIG. 6. (Color online) Components of the current density (in unit of $he/2ma$) calculated for α=5 and n=1. It shows that the particle moves along the lines $\mathbf{B}(\mathbf{r})=0$ indicated in black.

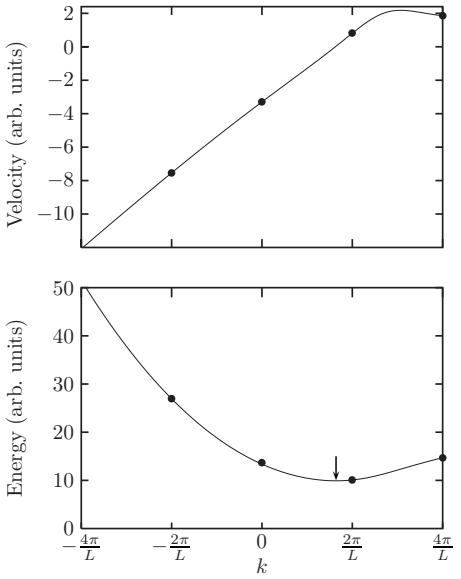

FIG. 7. (a) Schematic view of the velocity and (b) dispersion curves (only the first band is shown) of an electron moving in a linear magnetic field. When the line $B(\mathbf{r})=0$ is infinite, the energy spectrum is continuous as a function of momentum k along the line. The minimum at the dispersion is indicated by arrow, and it corresponds to $k_{\min}\neq 0$. For finite L the energy spectrum is discrete (black points).

pendicular to the lines $B(\mathbf{r})=0$. Similar oscillations were observed by Hofstetter *et al.*[16] for electrons moving in linear magnetic fields.

The appearance of persistent currents is due to the chirality of electron motion in the nonuniform magnetic field along the line of $B(\mathbf{r})=0$. One can understand it by using a semiclassical picture of the 1D motion in the inhomogeneous field.[15] The effective potential for the motion of an electron along the zero-field line is different for the opposite directions of the motion. It results in a strong asymmetry of the electron energy spectrum with respect to $k\rightarrow -k$, where k is the electron momentum along the zero-field line.

In the case of 2D periodic field, this chirality of electron energy spectrum should be combined with the fact that the trajectories are closed in circles. Then the energy spectrum is not only asymmetric but also quantized due to the quantization of the motion along the circular trajectory. Using the semiclassical picture, one can find the quantized values of the momentum from relation $k_n - A_l = 2\pi n/L$, where A_l is the vector potential along the contour and L is its length. The circulation of A_l along the circle is equal to the encompassed flux, which causes the difference in phases for electron motion in opposite directions. Thus, the condition of quantization can be also presented as $k_n = 2\pi(n+\phi/\phi_0)/L$. In our 2D model of periodic field, the ratio ϕ/ϕ_0 can be related to the parameter α. The calculation of flux through an isoline $B=0$ using Eq. (10) gives $\phi/\phi_0 \simeq 3.2437\alpha$.

Figure 7(b) shows schematically the energy spectrum as a function of momentum k along the circle. The points correspond to the quantized values of k. As we see from Fig. 7, even for integer values of ϕ/ϕ_0, i.e., in absence of the Aharonov-Bohm effect, the chirality of the motion in opposite directions would result in appearance of nonzero electric current along the circle. We therefore have identified a mechanism for appearance of the persistent currents.

V. HALL EFFECT IN THE PERIODIC MAGNETIC FIELD

Here we consider the occurrence of nonvanishing off-diagonal conductivity in the 2DEG with periodic magnetic field. As emphasized earlier, we assume that the average magnetic field is zero so that the ordinary Hall effect is absent. In our case, the mechanism of nonzero Hall conductivity has the same origin as the "intrinsic mechanism"[23,24,31] of the anomalous Hall effect in ferromagnets; i.e., the Hall effect in 2DEG in periodic magnetic field is related to the nontrivial *topology of electron energy bands* in the momentum space. However, unlike the anomalous Hall effect in ferromagnets, it does not require any uniform magnetization.

It should be noted that this effect is also quite different from the recently proposed "topological Hall effect" in textured ferromagnets.[6] Even though it was proposed in Ref. 6 to use the periodic magnetic field and 2D semiconductor with magnetic impurities, the only role of the magnetic field was to order the magnetic moments in correspondence to the field periodicity so that the topological properties of the magnetization profile are responsible for the topological Hall effect. But in the model under consideration there is no magnetization related to magnetic impurities. Nevertheless, as we can see from the calculation of the off-diagonal conductivity, σ_{xy}, the Hall effect is nonzero.

The occurrence of Hall effect and the quantization of Hall conductivity have been discovered in the past in the frame of 2D tight-binding honeycomb model with an additional periodic magnetic field.[32] The phase diagram of this model has two phases with Chern numbers ± 1. Also, the quantum Hall effect without any external magnetic field was found by Volovik[33] in the model of electrons in ^{3}He film. In both cases the origin of the Hall effect is related to topological properties of electron energy bands.

Assuming that the Fermi level is in the energy gap and in the absence of impurities one obtains from the Kubo formula,[23,24]

$$\sigma_{xy} = \frac{e^2}{\hbar}\sum_n \int \frac{d^2\mathbf{k}}{(2\pi)^2} f(\varepsilon_{n,\mathbf{k}})\Omega_{n,\mathbf{k}}, \tag{18}$$

where

$$\Omega_{n,\mathbf{k}} = \nabla_{\mathbf{k}} \times \mathcal{A}_{n,\mathbf{k}} \tag{19}$$

is the Berry curvature, $\mathcal{A}_{n,\mathbf{k}} = -i\langle n,\mathbf{k}|\nabla_{\mathbf{k}}|n,\mathbf{k}\rangle$ is the gauge connection, and $f(\varepsilon)$ is the Fermi function. Expression (18) was first found by Karplus and Luttinger[31] in the context of the anomalous Hall effect.

Thus, if the Fermi level is in the energy gap and the temperature is zero, the sum in Eq. (18) can be presented as a sum over fully occupied energy bands

$$\sigma_{xy} = \frac{e^2}{\hbar}\sum_n{}' \mathrm{Ch}_n, \tag{20}$$

where we denoted as,

$$\mathrm{Ch}_n = \int \frac{d^2\mathbf{k}}{(2\pi)^2}\Omega_{n,\mathbf{k}}, \tag{21}$$

the Chern number of the nth energy band. The Chern numbers are integer[34,35] because they are topological invariants.[36] Correspondingly, if the Fermi level is in the gap, the Hall conductivity [Eq. (20)] is quantized such as in case of the quantum Hall effect.[34] The value of σ_{xy} changes when the gap between two occupied bands is closing and depends explicitly on the dispersion relation around the points where the band degeneracies occur.[37,38] So, the calculation of the off-diagonal conductivity reduces to the calculations of the Chern numbers when the Fermi level is located between two separated bands.

We calculate numerically the Berry curvature [Eq. (19)] and the Chern numbers [Eq. (21)]. It should be noted that the computation of the derivative is a hard task because the phase of the Bloch state is ill defined and gauge dependent. Moreover, the summation over the first Brillouin zone involves a large number of $\mathbf{k}$ points. The problem of derivatives can be overcome by expressing the Berry connection in term of the matrix elements of the velocity operators,

$$\Omega_{n,\mathbf{k}} = i\sum_{m\neq n}\frac{v_x^{nm}v_y^{mn} - v_y^{nm}v_x^{mn}}{(\varepsilon_{n,\mathbf{k}} - \varepsilon_{m,\mathbf{k}})^2}, \tag{22}$$

where

$$\mathbf{v}^{nm} = \langle n,\mathbf{k}|\frac{\partial\mathcal{H}_\mathbf{k}}{\partial\mathbf{k}}|m,\mathbf{k}\rangle \tag{23}$$

are the off-diagonal elements of the velocity operator. This formula is gauge invariant but two difficulties remain. (i) We need to calculate the sum over all energy bands and (ii) the computational efforts to calculate the elements of the velocity operator can still be important. In practice, the summation over unoccupied bands is usually truncated over a few number of unoccupied bands but a large number of $\mathbf{k}$ point is still needed to calculate the Chern numbers.

Recently, Fukui *et al.*[39] proposed another method of calculation of the Chern numbers. This method has some advantages: one needs to calculate only the Bloch states of occupied bands over a coarse mesh of the first Brillouin zone. Moreover, the method is gauge invariant. In order to calculate the Chern numbers, we define the quantity

$$\gamma_\mathcal{P}^n = \mathrm{Im}\,\log(\langle n,\mathbf{k}_1|n,\mathbf{k}_2\rangle\langle n,\mathbf{k}_2|n,\mathbf{k}_3\rangle \times \langle n,\mathbf{k}_3|n,\mathbf{k}_4\rangle\langle n,\mathbf{k}_4|n,\mathbf{k}_1\rangle), \tag{24}$$

where the function $\log z$ is defined in the complex plane with branch cut along the negative real axis and $\mathcal{P}_s$ is a small closed path passing by the points $\mathbf{k}_s$ with $s=1,2,3,4$. The quantity $\gamma_\mathcal{P}^n$, which is often called the field strength, is the Berry phase that a Bloch state acquires when it is transported adiabatically along the path $\mathcal{P}_s$. In this formalism, the Chern number is given by a sum over the coarse mesh of phases $\gamma_{\mathcal{P}_s}^n$,

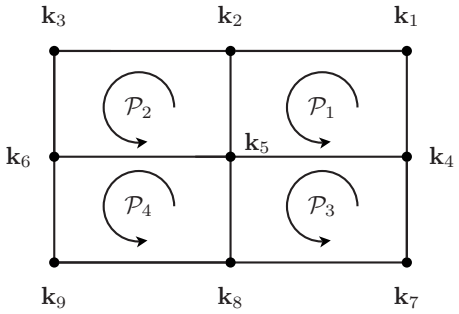

FIG. 8. Principle of construction of the paths $\mathcal{P}_s$ in the case of a rectangular Brillouin zone and a given mesh. The black points indicate the mesh taken for the decomposition of the first Brillouin zone. $\mathcal{P}_1=\mathbf{k}_1\rightarrow\mathbf{k}_2\rightarrow\mathbf{k}_5\rightarrow\mathbf{k}_4\rightarrow\mathbf{k}_1$ and the orientation is indicated by the arrow inside the rectangle. The others paths can be easy deduced using a similar construction.

$$\mathrm{Ch}_n = \sum_{\mathcal{P}_s}\gamma_{\mathcal{P}_s}^n. \tag{25}$$

The last step is to decompose the first Brillouin zone into small paths $\mathcal{P}_s$ and to calculate the field strength $\gamma_{\mathcal{P}_s}^n$ for each small path. The decomposition of the first Brillouin zone is illustrated in Fig. 8.

We calculated the Chern numbers of the first five energy bands of our problem using this method and obtained the results, which are shown in Fig. 9. It should be noted that the sum given by Eq. (25) depends strongly on the number of plane waves used to calculate the solutions of the Schrödinger equation. This phenomena, which is not related to any numerical errors, occurs because the truncation of the basis breaks the symmetry $\mathcal{H}_{\mathbf{k}+\mathbf{g}}=\mathcal{H}_\mathbf{k}$, where $\mathbf{g}$ is a vector of the reciprocal space.[40] The latter relation is used to prove that the off-diagonal conductivity is an integer when the Fermi level is in the gap. This effect cannot be observed in the case of tight-binding models because this symmetry is always verified. The effect disappears quickly when the number of plane waves is increasing.

The Chern numbers of the first five bands are presented in Fig. 9. These results show that the variation in the Chern numbers with the intensity of field looks rather chaotic and there is no simple relation between the values of α, for which the band crossing occurs. It is known that the Chern numbers are related to the band crossings between the different bands.[41] The value of the jump depends on the number of k points in the first Brillouin zone, where the band crossing occurs, and the dispersion relation around these points.[38] Although the physical mechanism is essentially the same, the behavior observed here is much more complex as the one obtained in Haldane's simplified model.[26]

According to Eq. (20) the Hall conductivity can be found using the Chern numbers provided that the Fermi energy is within the gap. The dependence of σ_{xy} on α is presented in Fig. 10 for several integer numbers of electrons per unit cell n. The solid line corresponds to the location of Fermi level within the energy gap. The gap opens between closest bands when α is increased. Each plateau demonstrates quantization of the Hall conductivity within an interval of α.

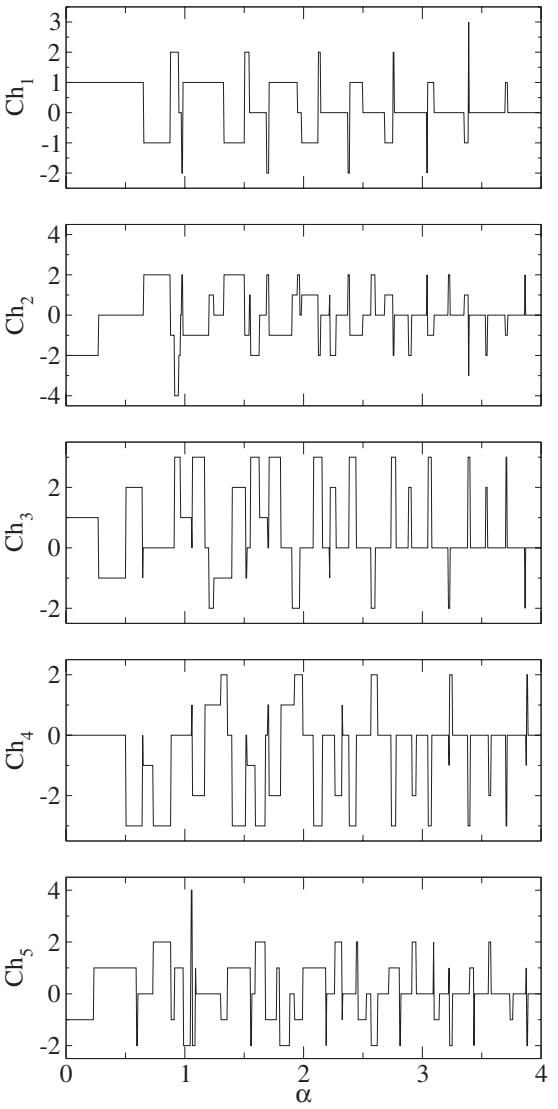

FIG. 9. Chern numbers of the first energy bands calculated as a function of the amplitude of the magnetic field α. This figure shows that the Chern numbers have chaotic variations which are connected to closing gaps between the different bands.

In the other intervals of α, the energy bands are overlapping as we can see in Fig. 2. In this case the Fermi level is crossing the electron bands, and the Hall conductivity cannot be expressed by the Chern numbers of separated bands. We show it in the figure by the dotted line.

For large magnetic fields, $\alpha \gg 1$, we found that the Hall conductivity vanishes as the Chern numbers tend to zero when α is increasing (Fig. 9). This is due to the fact that for large values of α the electrons are strongly localized on the lines of zero field as discussed in Sec. III C.

Our result confirms that the off-diagonal conductivity is quantized if the Fermi level is located within the gap. It should be noted that this does not really prove the existence of Hall plateau, which could be observed when the field amplitude is varied for ideal systems. However, as for the usual quantum Hall effect, the existence of finite plateaus with quantized Hall conductivity, as α or electron density is varied, will result from the formation of strongly localized states in mobility gaps due to disorder and impurity scattering.

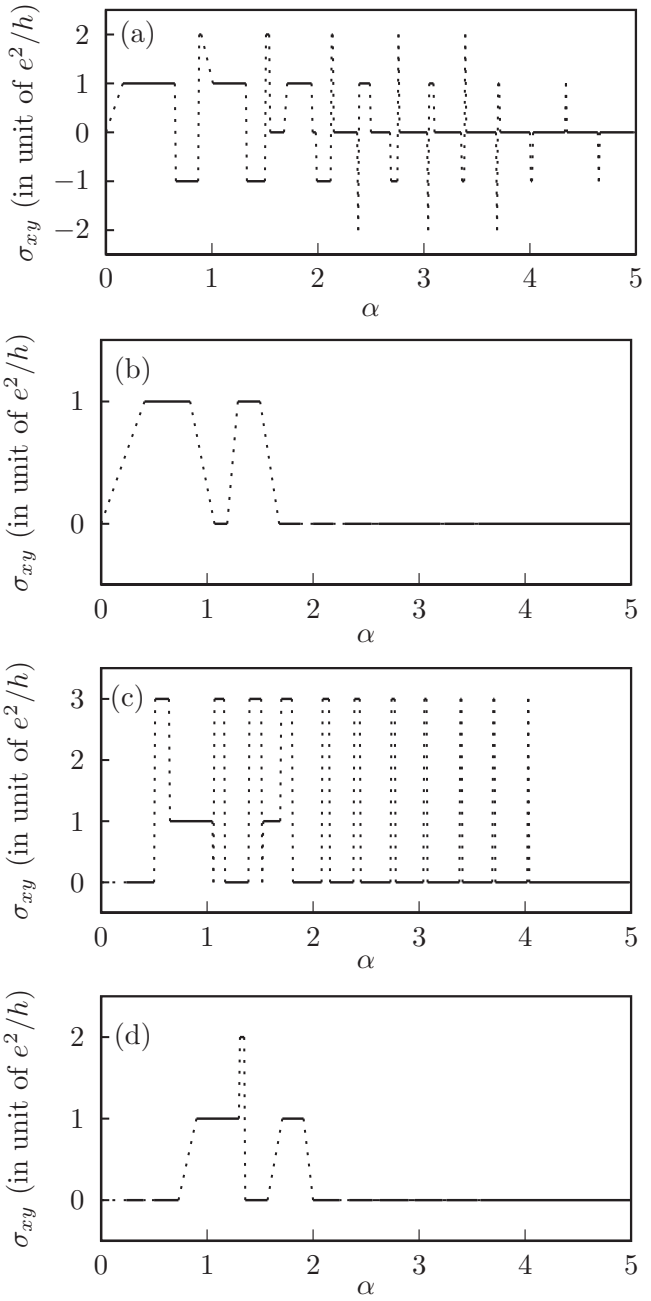

FIG. 10. Anomalous Hall conductivity as a function of α for different numbers of electrons per unit cell (a) $n=1$, (b) 2, (c) 3, and (d) 4. The solid line corresponds to the Fermi level within the gap, and this demonstrates quantization of the anomalous Hall conductivity.

VI. EFFECT OF ELECTRON SPIN

In the previous consideration we did not take into account the spin of electron. Now we discuss the effect of Zeeman coupling between the electron spin and magnetic field. We show that in the case of strong magnetic field it leads to a small correction of vector potential.

We consider the following Hamiltonian:

$$\mathcal{H} = \frac{1}{2m}[-i\hbar\nabla - q\mathbf{A}(\mathbf{r})]^2 + g\mu_B\mathbf{B}(\mathbf{r})\cdot\boldsymbol{\sigma}, \tag{26}$$

where g is the gyromagnetic constant, μ_B is the Bohr magneton, and $\boldsymbol{\sigma}$ are the Pauli matrices. It should be noted that μ_B is determined by the mass of free electron, m_0, whereas the first term in Eq. (26) contains the effective mass m. In the case of semiconductors such as, e.g., GaAs, the large difference of these masses, $m/m_0 \ll 1$, leads to relatively small Zeeman splitting.

After a local rotation $\mathcal{T}(\mathbf{r})$ of the quantization axes along the field in each point, the Hamiltonian reads

$$\mathcal{H} = \frac{1}{2m}[-i\hbar\nabla - q\mathbf{A}(\mathbf{r}) - q\mathbf{A}_g(\mathbf{r})]^2 + g\mu_B|\mathbf{B}(\mathbf{r})|\sigma_z, \tag{27}$$

with

$$\mathbf{A}_g(\mathbf{r}) = -\frac{i\hbar}{q}\mathcal{T}^\dagger(\mathbf{r})\,\nabla\,\mathcal{T}(\mathbf{r}) = \mathbf{A}_g^x\sigma_x + \mathbf{A}_g^y\sigma_y + \mathbf{A}_g^z\sigma_z. \tag{28}$$

The gauge field $\mathbf{A}_g(\mathbf{r})$ depends only on unit vector $\mathbf{n}(\mathbf{r}) = \mathbf{B}(\mathbf{r})/|\mathbf{B}(\mathbf{r})|$ which represents the direction of field in point $\mathbf{r}$. In the adiabatic regime, the off-diagonal terms of the gauge field $\mathbf{A}_g(\mathbf{r})$ can be neglected.[6] Hence, the spin-up and spin-down electrons are decoupled, and the effective Hamiltonian describing each species have a form of Eq. (1) where the effective magnetic field is given by $\mathbf{B}(\mathbf{r}) = \mathbf{B}_z(\mathbf{r}) \pm \mathbf{B}_g(\mathbf{r})$, with $\mathbf{B}_g(\mathbf{r}) = \nabla \times \mathbf{A}_g^z(\mathbf{r})$.

The gauge field $\mathbf{B}_g(\mathbf{r})$ depends only on geometry of the magnetic lattice but does not depend on the amplitude of field $\mathbf{B}(\mathbf{r})$.[6] Its flux is quantized and equal to $2\pi n\phi_0$ with $n \in \mathbb{Z}$. Then the gauge field $\mathbf{B}_g(\mathbf{r})$ can be neglected if the amplitude of magnetic field $\mathbf{B}(\mathbf{r})$ is larger than $2\pi n\phi_0/S$ or, in other terms, if $\alpha \gg 1$.

VII. CONCLUSIONS

We calculated the energy spectrum of 2D electron gas in periodic field with the symmetry of triangular lattice. As we can see, the energy-band structure can be controlled by the variation in the magnetic-field strength. Using the realistic parameters of Fe nanolattice with the lattice parameter of 100 nm, we have estimated the magnitude of magnetic field as 5 kG,[6] which corresponds to values of α of the order of 0.1. This value strongly depends on the gap between the nanolattice and the electron gas, which gives a possible way to vary the field strength.

As a 2D electron gas one can use a metallic or semiconductor layer. In this case there is also an additional crystal-lattice field but the corresponding lattice constant a_0 is much smaller that the lattice constant of the periodic magnetic field a. It means that we can neglect the effect of periodic field of the crystal lattice as long as the energy of electrons $\varepsilon \ll \hbar^2/ma_0^2$.

We found that the low-energy electrons are effectively localized near the lines of zero magnetic field, and in this state they produce an equilibrium persistent currents in form of a ring array. The mechanism of creation of such persistent currents is not necessarily induced by the magnetic flux through the ring but is rather related to the peculiarities of electron motion in opposite directions along the zero-field lines.

We have also shown that the quantum Hall effect can be observed in this system when the Fermi energy is located in the gap. In principle, the problem of controlling the Fermi-level location has been already solved for 2D system with the gate. In a structure with fully controlled periodic magnetic field and the Fermi energy, it would result in a large functionality of the structure.

It should be noted that the impurity effects have been ignored in our calculations. This is justified if the characteristic sizes of 2D structure are smaller than the electron mean-free path.

ACKNOWLEDGMENTS

This work was supported by the FCT under Grant No. PTDC/FIS/70843/2006 in Portugal, Polish Ministry of Science and Higher Education as research projects in years 2006–2009 and 2007–2010, and by the STCU under Grant No. 3098 in Ukraine. V.D. thanks MPI für Mikrostrukturphysik in Halle and the Institut Néel, CNRS/UJF, in Grenoble for the hospitality.

[1] K. Nielsch, R. B. Wehrspohn, J. Barthel, J. Kirschner, U. Gösele, S. F. Fischer, and H. Kronmüller, Appl. Phys. Lett. **79**, 1360 (2001); K. Nielsch, R. B. Wehrspohn, J. Barthel, J. Kirschner, S. F. Fischer, H. Kronmüller, T. Schweinböck, D. Weiss, and U. Gösele, J. Magn. Magn. Mater. **249**, 234 (2002).

[2] J. Ye, Y. B. Kim, A. J. Millis, B. I. Shraiman, P. Majumdar, and Z. Tesanovic, Phys. Rev. Lett. **83**, 3737 (1999).

[3] G. Tatara and H. Kawamura, J. Phys. Soc. Jpn. **71**, 2613 (2002); H. Kawamura, Phys. Rev. Lett. **90**, 047202 (2003).

[4] Y. Taguchi and Y. Tokura, Europhys. Lett. **54**, 401 (2001); Y. Taguchi, Y. Oohara, H. Yoshizawa, N. Nagaosa, and Y. Tokura, Science **291**, 2573 (2001); Y. Taguchi, T. Sasaki, S. Awaji, Y. Iwasa, T. Tayama, T. Sakakibara, S. Iguchi, T. Ito, and Y. Tokura, Phys. Rev. Lett. **90**, 257202 (2003).

[5] S. Onoda and N. Nagaosa, Phys. Rev. Lett. **90**, 196602 (2003); S. Onoda, N. Sugimoto, and N. Nagaosa, *ibid.* **97**, 126602 (2006).

[6] P. Bruno, V. K. Dugaev, and M. Taillefumier, Phys. Rev. Lett. **93**, 096806 (2004).

[7] A. V. Silhanek, W. Gillijns, M. V. Milosević, A. Volodin, V. V. Moshchalkov, and F. M. Peeters, Phys. Rev. B **76**, 100502(R) (2007).

[8] I. S. Ibrahim and F. M. Peeters, Phys. Rev. B **52**, 17321 (1995).

[9] B. Y. Gu, W. D. Sheng, X. H. Wang, and J. Wang, Phys. Rev. B

56, 13434 (1997).
[10] D. P. Xue and G. Xiao, Phys. Rev. B **45**, 5986 (1992).
[11] A. Krakovsky, Phys. Rev. B **53**, 8469 (1996).
[12] Q. W. Shi and K. Y. Szeto, Phys. Rev. B **55**, 4558 (1997); **56**, 9251 (1997).
[13] M. C. Chang and Q. Niu, Phys. Rev. B **50**, 10843 (1994); M. C. Chang and M. F. Yang, *ibid.* **57**, 13002 (1998).
[14] A. Y. Rom, S. Fishman, R. Kosloff, and T. Maniv, Phys. Rev. B **54**, 9819 (1996); A. Y. Rom, *ibid.* **55**, 11025 (1997).
[15] J. E. Müller, Phys. Rev. Lett. **68**, 385 (1992).
[16] E. Hofstetter, J. M. C. Taylor, and A. MacKinnon, Phys. Rev. B **53**, 4676 (1996).
[17] B. Büttiker, Y. Imry, and R. Landauer, Phys. Lett. **96A**, 365 (1983); R. Landauer and M. Büttiker, Phys. Rev. Lett. **54**, 2049 (1985).
[18] H. F. Cheung, Y. Gefen, E. K. Riedel, and W. H. Shih, Phys. Rev. B **37**, 6050 (1988).
[19] B. L. Altshuler, Y. Gefen, and Y. Imry, Phys. Rev. Lett. **66**, 88 (1991).
[20] D. Loss and P. Goldbart, Phys. Rev. B **43**, 13762 (1991).
[21] S. Fujimoto and N. Kawakami, Phys. Rev. B **48**, 17406 (1993).
[22] G. H. Ding and B. Dong, Phys. Rev. B **76**, 125301 (2007).
[23] T. Jungwirth, Q. Niu, and A. H. MacDonald, Phys. Rev. Lett. **88**, 207208 (2002); D. Culcer, A. MacDonald, and Q. Niu, Phys. Rev. B **68**, 045327 (2003); T. Jungwirth, J. Sinova, K. Y. Wang, K. W. Edmonds, R. P. Campion, B. L. Gallagher, C. T. Foxon, Q. Niu, and A. H. MacDonald, Appl. Phys. Lett. **83**, 320 (2003); D. Culcer, J. Sinova, N. A. Sinitsyn, T. Jungwirth, A. H. MacDonald, and Q. Niu, Phys. Rev. Lett. **93**, 046602 (2004).
[24] M. Onoda and N. Nagaosa, J. Phys. Soc. Jpn. **71**, 19 (2002); Phys. Rev. Lett. **90**, 206601 (2003); Z. Fang, N. Nagaosa, K. S. Takahashi, A. Asamitsu, R. Mathieu, T. Ogasawara, H. Yamada, M. Kawasaki, Y. Tokura, and K. Terakura, Science **302**, 92 (2003).
[25] G. Sundaram and Q. Niu, Phys. Rev. B **59**, 14915 (1999).
[26] F. D. M. Haldane, Phys. Rev. Lett. **93**, 206602 (2004).
[27] Y. Yao, L. Kleinman, A. H. MacDonald, J. Sinova, T. Jungwirth, D. S. Wang, E. Wang, and Q. Niu, Phys. Rev. Lett. **92**, 037204 (2004).
[28] X. Wang, J. R. Yates, I. Souza, and D. Vanderbilt, Phys. Rev. B **74**, 195118 (2006).
[29] M. Taillefumier, B. Canals, C. Lacroix, V. K. Dugaev, and P. Bruno, Phys. Rev. B **74**, 085105 (2006).
[30] V. Hernandez, J. E. Roman, and V. Vidal, ACM Trans. Math. Softw. **31**, 351 (2005).
[31] R. Karplus and J. M. Luttinger, Phys. Rev. **95**, 1154 (1954).
[32] F. D. M. Haldane, Phys. Rev. Lett. **61**, 2015 (1988).
[33] G. E. Volovik, Zh. Eksp. Teor. Fiz. **94**, 123 (1988) [Sov. Phys. JETP **67**, 1804 (1988)].
[34] D. J. Thouless, M. Kohmoto, M. P. Nightingale, and M. den Nijs, Phys. Rev. Lett. **49**, 405 (1982).
[35] Q. Niu, D. J. Thouless, and Y. S. Wu, Phys. Rev. B **31**, 3372 (1985).
[36] They are known in topology as the first Chern classes of a $U(1)$ principal fiber bundle of the ground-state wave functions on the base manifold of a torus T^2 (Ref. 35).
[37] Y. Hatsugai, Phys. Rev. Lett. **71**, 3697 (1993); Phys. Rev. B **48**, 11851 (1993).
[38] M. Oshikawa, Phys. Rev. B **50**, 17357 (1994).
[39] T. Fukui, Y. Hatsugai, and H. Suzuki, J. Phys. Soc. Jpn. **74**, 1674 (2005).
[40] R. B. Laughlin, Phys. Rev. B **23**, 5632 (1981); B. I. Halperin, *ibid.* **25**, 2185 (1982); D. R. Yennie, Rev. Mod. Phys. **59**, 781 (1987).
[41] M. V. Berry, Proc. R. Soc. London, Ser. A **392**, 45 (1984).